energies

MDPI

Article

Experimental Study and Optimisation of a Non-Conventional Ignition System for Reciprocating Engines Operation with Hydrogen–Methane Blends, Syngas, and Biogas

Luigi De Simio [1], Sabato Iannaccone [1], Massimo Masi [2] and Paolo Gobbato [3,*]

[1] Institute of Sciences and Technologies for Sustainable Energy and Mobility, National Research Council, 80125 Napoli, Italy
[2] Department of Management and Engineering—DTG, University of Padova, 36100 Vicenza, Italy
[3] Veil Energy Srl SB, 39100 Bolzano, Italy
* Correspondence: p.gobbato@veil-energy.eu

Abstract: The paper deals with the experimental study of a medium-load spark ignition engine under operation with different fuel mixtures among those deemed as promising for the transition towards carbon-free energy systems. In particular, the performance of a non-conventional ignition system, which permits the variation of the ignition energy, the spark intensity and duration, was studied fuelling the engine with 60–40% hydrogen–methane blends, three real syngas mixtures and one biogas. The paper is aimed to find the optimal ignition timing for minimum specific fuel consumption and the best setup of the ignition system for each of the fuel mixtures considered. To this end, a series of steady-state tests were performed at the dynamometer by varying the parameters of the ignition system and running the engine with surrogate hydrogen–methane–nitrogen mixtures that permit the simulation of hydrogen–methane blends, real syngas, and biogas. The results quantify the increase of spark advance associated with the decrease of the fuel quality and discuss the risk of knock onset during methane–hydrogen operation. It was demonstrated that the change of the ignition system parameters does not affect the value of optimum spark advance and, except for the ignition duration, all the parameters' values are generally not very relevant at full load operation. In contrast, at partial load operation with low-quality syngas or high exhaust gas recirculation rate, it was found that an increase of the maximum ignition energy (to 300 mJ) allows for operation down to approximately 66% of the maximum load before combustion becomes incomplete. Further reductions, down to 25% of the maximum load, can be achieved by increasing the gap between the spark plug electrodes (from 0.25 to 0.5 mm).

Keywords: syngas; hydrogen; biogas; ignition energy; spark duration; spark intensity

Citation: De Simio, L.; Iannaccone, S.; Masi, M.; Gobbato, P. Experimental Study and Optimisation of a Non-Conventional Ignition System for Reciprocating Engines Operation with Hydrogen–Methane Blends, Syngas, and Biogas. *Energies* **2022**, *15*, 8270. https://doi.org/10.3390/en15218270

Academic Editor: Jamie W.G. Turner

Received: 26 September 2022
Accepted: 26 October 2022
Published: 5 November 2022

1. Introduction

In the pathway towards a 100% decarbonised global energy system, internal combustion engines (ICEs) will progressively leave the traditional liquid fuels to be eventually fuelled by "green" hydrogen, at least in those niches where technological alternatives seem far to be available. Whatever the speed of this transition and the corresponding evolution of the amplitude of those niches, the onset of a "transitional fuels" scenario is reasonable. In this scenario, syngas derived from biomasses, biogas, and hydrogen–methane mixtures will play some role. In particular, hydrogen–methane mixtures could become of interest if the natural gas (NG) network will be used to accommodate some amount of hydrogen, as discussed in Danieli et al. [1]. Hydrogen–methane mixtures, syngas, and biogas fuels share some common features but also present some peculiar characteristics, which are briefly summarized in the following.

"Green" hydrogen, i.e., hydrogen obtained by electrolysers powered with current from renewable sources, has the potential to become a valid alternative to conventional

fuels both in transportation and cogeneration plants, if the hydrogen agenda planned by several countries will be kept in the near future (see, e.g., the Hydrogen roadmap Europe report [2]). In fact, hydrogen can be efficiently oxidized in fuel cells, or it could be burnt in ICEs with lower efficiency but less cost. Hydrogen is also one of the components of syngas, a mixture of combustible gases diluted in a high concentration of inert species. In addition to H_2, the syngas combustible fraction includes carbon monoxide, traces of CH_4, and heavier hydrocarbons. Instead, most of the inert components are CO_2, nitrogen, water vapour, and various impurities, such as dust and tars. The raw materials for syngas production are treated through gasification or pyrolysis processes. The gasification process, which consists of the partial oxidation of a solid, liquid or gaseous substance in a high-temperature environment (900–1100 °C), includes three phases: a first of highly exothermic combustion, a second of pyrolysis, and finally, the conversion of carbon into gaseous compounds. Syngas composition presents a variability that depends on the biomass used and the specific gasification technology involved. For the most diffused air-gasification plants, the lower calorific value (LHV) of the produced syngas is quite low and varies in the range of 4–7 MJ/Nm^3 [3]. Higher LHVs, in the range from 10 to 18 MJ/Nm^3, are obtained by oxygen gasifiers [4]. This technology requires feeding the gasifier with homogeneous material to increase the efficiency of the process. Moreover, a subsequent purification phase is essential to remove tars and chars from the produced gas. Biogas shares with syngas the high inert content characteristic: its combustible fraction is almost completely constituted by CH_4, whereas the inert fraction is mostly CO_2 with a small amount of moisture. Biogas is produced by means of anaerobic digesters, biodigesters or bioreactors. It may contain a small percentage of hydrogen sulphide and siloxanes. As for H_2 from renewables, syngas and biogas can contribute to the reduction of GHG emissions if agricultural waste or biomass from short-rotation forestry are used as feedstock for its production.

The use of these "transitional fuels" to power ICEs offers opportunities related to some interesting features of these fuels, but also proposes some technical issues that should be addressed. In particular, difficulties of charge ignition and combustion completion and stability are issues usually of relevant importance when non-conventional fuels are considered. In the next three paragraphs such aspects are briefly reviewed in the light of the scientific literature findings.

Hydrogen-methane ICEs. The use of pure hydrogen allows for an efficient lean combustion but, compared to liquid fuels, reduces the kilometric range of ICE-vehicles for transportation more than the use of natural gas does. In fact, the lower energy density of hydrogen is not counterbalanced by an increase of pressure in the fuel tanks. This results in approximately 70% reduction of the kilometric range if compared to that assured by pure methane. Furthermore, the issue of hot spots pre-ignition phenomena is amplified by the lower ignition energy of H_2 in air (about a tenth of that of methane [5]). The pre-ignition, unlike knocking, cannot be controlled only with the ignition timing, but requires substantial modifications of the combustion chamber design. On the contrary, the use of H_2–methane or H_2–NG mixtures containing H_2 between 10 and 30% by volume does not require substantial modifications of the existing natural gas engines and ensures a sensible increase of the turbulent flame front speed propagation [6,7]. High flame speeds give more complete and stable combustion, although higher NO_x emissions must be expected [8].

Syngas-fuelled ICEs. These engines burn in premixed mode an air–syngas mixture, whose combustion is triggered by the compression ignition of a small pilot fuel injection—in the dual-fuel (DF) compression ignition (CI) engines—and by a spark plug—in spark ignition (SI) engines. The syngas fuelling has aspects resembling to dilution of the intake charge with exhaust gas recirculation (EGR), due to the shared characteristic of a high concentration of inert species. However, in the case of EGR technology, it is possible to modify the fraction of exhaust gas recycled as a function of the engine operating conditions. It is also possible to mitigate the negative effect of inert gasses on the burning rate by means of either early injection advances—in the case of CI engines [9]—or higher ignition advances—in the case of SI engines [10]. In contrast, in the case of syngas fuelling, the

flexibility in controlling the concentration of inert species is not feasible and it is therefore essential to optimize the ignition phase. In DF engines, the ignition phase takes place without difficulties since the self-ignition of the pilot fuel is easy to achieve, but knock and incomplete combustion can arise at high and low load, respectively. Therefore, the optimization of the DF engine combustion process mainly concerns the pilot-fuel injection phase and the syngas to pilot-fuel ratio. These two parameters should be both modified as a function of the engine working point because the concentration of inert gasses entering the engine varies as the syngas amount does. In relation to that issue, Costa et al. [11] conducted a combined experimental-numerical investigation in which they optimized the pilot injection of a vegetable fuel so that they were able to run the engine with reliable performance up to high percentages of syngas fuel. In SI engines, the syngas to air-flow rate ratio can vary in a narrow range. However, moving from a stoichiometric to a lean fuel–air mixture allows a certain control of the inert share as a function of the engine load and speed. On the other hand, the air excess sums to the effect of the inert gasses in slowing down the speed of combustion and increasing the difficulties to precisely control the ignition phase. Thus, the main difficulty lies in ensuring the proper ignition of the mixture and the effective propagation of the resulting flame front. Some years ago, Gamiño et al. [12] numerically studied the use of a multi-spark ignition system to compensate for the low flame speed. More recently, Jang et al. [13] and Wang et al. [14] studied the optimization of the ignition advance on engines burning syngas obtained from methanol and water, and syngas and biogas produced from horticultural wastes, respectively.

Biogas-fuelled ICEs. Biogas can be used in ICEs in a very similar way compared to syngas, since it only requires different values of the control parameters to manage the concentration of combustible gases with respect to inert species (i.e., the content of CH_4 with respect to CO_2).

In spite of this similarity, there are substantial review studies (e.g., [15,16]) which lead to deduce that the quantitative role of ignition energy on low LHV fuel-powered engines has not yet been sufficiently investigated.

The issues briefly summarised above highlight that ignition systems may play an important technical role during the transition towards a 100% renewable energy economy, because of their capability to extend the stable operation of ICEs fed with non-conventional fuels. In fact, a reliable ignition of traditional fossil fuels occurs with spark energy and duration on the order of 50 mJ and 0.5 ms, respectively, also in the most unfavourable operating conditions of the engine (see, e.g., Heywood [17]). Instead, the ignition of non-conventional fuels, and mostly those containing a very limited amount of fossil fuels in their mix, may be difficult also in the usual operating range of the engine. This justifies the development of non-conventional ignition systems, i.e., those able to significantly exceed the values of the spark energy and duration listed above.

The aim of this paper is to experimentally analyse the performance and the optimum setup of a non-conventional ignition system applied to a medium-load SI engine fuelled with different syngas mixtures, one biogas fuel and a H_2–CH_4 mixture with 60% volume H_2 content. To this end, the engine, originally conceived for natural gas operation, was modified in its fuel system (to allow operation with several H_2–CH_4–N_2 fuel blends) and in its ignition system (to extend as much as possible the operation with such fuel blends). Note that for the test bench activity with syngas fuels, most of studies available in the literature used surrogate mixtures instead of the actual fuels. In fact, due to their simplified composition, surrogate fuel mixtures make the tests' repeatability easier, which is difficult to be assured if the engine is directly fuelled by the biomass-dependent gasifier product. For example, Bhaduri et al. [18] and Nadaleti et al. [19] used a five-species mixture made of CO, H_2, and CH_4 with the addition of N_2 and CO_2 as inert species. Instead, Park et al. [20] simulated syngas with ternary mixtures of H_2, CO, and CO_2. On the other hand, surrogate mixtures may avoid safety concerns during the testing activity related to the toxicity of carbon-monoxide present in real syngas fuels. Therefore, the experimental activity of the present study was carried out using surrogate mixtures, which do not contain CO and

are made of H_2, CH_4, and N_2, with a composition defined in accordance with the method suggested by the authors in a previous work [21].

The paper is organised as follows: first, the modification to the intake system design is theoretically discussed. Then, the three real syngas mixtures, the biogas fuel, and the hydrogen–methane blend are presented and reduced to their corresponding surrogate mixtures composed by H_2–CH_4–N_2. The last part of the manuscript deals with the experimental activities and includes the description of the test rig with special attention to the ignition system, the presentation of the experimental measurements, and the critical discussion of results.

The novelty contribution of this work is twofold. From the fundamental research point of view, it is the first study in the literature analysing the effect of ignition parameters (spark energy and duration) or spark plug features (electrodes gap) on the performance of a specific stock production engine fed with different fuels. From the technical-practical point of view, it makes available to the community new sets of experimental data on a stock production engine fed with non-conventional fuels, which could be used in the very next future.

2. Engine Design Modifications

Two key issues must be considered to adapt an engine designed for conventional gaseous fuel (i.e., compressed natural gas—CNG) to syngas operation: (i) the change expected for the maximum engine power and (ii) the resizing of the engine intake and of the fuel-feeding systems required to allow for the admission of a fuel with a high inert content.

For a given reciprocating engine of displacement V [m^3] and fuel delivery in the intake manifold, the maximum achievable power is:

$$P = \frac{V \cdot n}{\varepsilon \cdot 60} \cdot \eta_{v,mix} \cdot LHV_{s,mix} \cdot \eta_f \quad (1)$$

where n is the engine speed (rpm), $\eta_{v,mix}$ is the volumetric efficiency based on the entire charge flow rate (air and fuel), η_f is the overall fuel conversion efficiency, ε is the number of engine revolutions for one power stroke, $LHV_{s,mix}$ is the energy content per unit volume of the stoichiometric mixture processed by the engine (kJ/m^3).

Assuming that η_f and $\eta_{v,mix}$ are not dependent on the fuel composition, it is possible to estimate the minimum change of the maximum power output of a specific engine due to the change of the gaseous fuel. The following numerical example could help to clarify that statement. The LHV_{syngas} of a syngas with a dry-based composition as that shown in Table 1 is equal to 7.73 MJ/Nm^3 at 0 °C and 1 bar (the value can be easily calculated by the volume-weighted addition of the LHV of each combustible species).

Table 1. Representative composition of a syngas on a dry basis.

Gas	[% vol.]
CO	26.0
CH_4	5.7
H_2	22.3
N_2	34.1
CO_2	11.9

The $LHV_{s,mix}$ of this syngas is equal to 2.86 MJ/Nm^3 and it is calculated taking into account the energy contained in the syngas unit volume and the total volume of the air–fuel mixture in stoichiometric conditions, as:

$$LHV_{s,mix} = \frac{LHV_{syngas}}{\alpha_{vs} + 1} \quad (2)$$

where α_{vs} is the volumetric air to fuel ratio evaluated under stoichiometric conditions, which is equal to 1.70 for the syngas in Table 1. The α_{vs} is calculated from the O_2 demand for each combustible component.

Thus, compared to pure methane which has $LHV_{s,mix}$ equal to 3.39 MJ/Nm^3, this syngas permits to achieve a maximum power that is approximately 16% lower. The reason is the lower α_{vs} value of the syngas (1.70 against 9.52 of the pure methane) which does not compensate for the large difference in *LHV* of the two fuels. In addition, it has to be taken into account that an engine designed for methane operation, if fuelled with the syngas of Table 1, cannot give the maximum expected power from the previous calculations, unless the original intake system is properly modified. Indeed, the volume of this syngas is on the same order of magnitude of the air required for its combustion, while the volume of methane is about one order of magnitude lower.

Under the assumption that the thermal and heat transfer effects dependent on the fuel composition are negligible, the size of the intake system can be calculated taking into account X_a, defined as the ratio between the volumes of air necessary to burn a unit volume of fuel in stoichiometric conditions and the total volume processed by the engine:

$$X_a = \frac{\alpha_{vs}}{\alpha_{vs} + 1} \tag{3}$$

Figure 1 plots X_a (expressed as a percentage) as a function of α_{vs}. On the trend line, the values for some fuels are marked with different symbols. It is evident that passing from methane to the syngas of Table 1, the value of X_a drops to about 50%. Therefore, in the most realistic hypothesis of fuel injection in the intake manifold, the section of the fuel ducts becomes comparable with the one engaged by the air. Accordingly, the overall intake system section and the engine displacement and/or turbocharging must be approximately doubled to obtain the maximum power achievable from the syngas considered in the example.

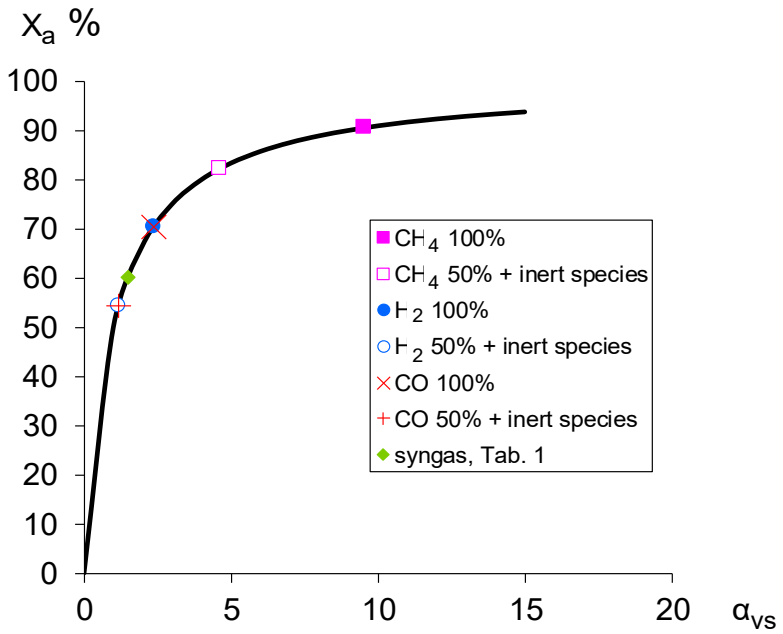

Figure 1. Trend of X_a as a function of α_{vs}.

3. Calculation of the Fuel Mixtures

The dry-based composition of the three syngas mixtures and one biogas considered in this study and derived from real applications are listed in Table 2. The table also includes in the last column the composition assumed for a hypothetical "transition fuel" (TF hereafter) made of green H_2 and green CH_4. Note that TF includes 13% N_2 and 1% CO_2 concentration,

which corresponds to approximately 3.5% mass concentration of exhaust gas recirculation at the engine intake. This EGR amount is assumed to be sufficient to avoid abnormal combustion in an SI engine originally designed for natural gas combustion when operating at full load.

Table 2. Composition and related properties of the real syngas mixtures, biogas, and transition fuel chosen for this study on a dry basis, at 15 °C and 1 bar.

Species	MIX R1	MIX R2	MIX R3	Biogas	TF
CO [% vol.]	23.9	18	29	0	0
CH_4 [% vol.]	1.6	2	2	64	34
H_2 [% vol.]	18.5	16	10.2	2	52
N_2 [% vol.]	44	52	37.3	0	13
O_2 [% vol.]	0	0	1.6	0	0
CO_2 [% vol.]	12	12	19.9	34	1
LHV [MJ/m^3]	5.3	4.5	5.2	21.9	16.8
$LHV_{s,mix}$ [MJ/m^3]	2.4	2.2	2.4	3.1	3.1
X_a [%]	54	50	53	88	82

As stated in Introduction, three-species surrogate mixtures made of hydrogen, methane, and nitrogen were used. Their compositions were specifically defined to simulate the three real syngas fuels of Table 2 according to the method suggested by Gobbato et al. [21]. The method states that a surrogate mixture must allow the engine to achieve the same power output and fuel conversion efficiency as when the engine is fuelled with the real syngas. This is assured when the stoichiometric $LHV_{s,mix}$ and the laminar flame speed (S_L) values of the surrogate fuel are equal to the corresponding property values of the real syngas fuel. Note that $LHV_{s,mix}$ is the heat release achievable from combustion and S_L is the parameter mostly affecting the combustion duration at specified load, speed, and thermal regime of the engine. In the method, S_L was considered in place of the turbulent flame velocity because: (i) it was assumed that turbulence has the same effect on the combustion kinetics of all the fuel species included in the mixtures, and (ii) turbulent velocity data are not available in the literature due to the difficulty in their experimental determination in the different conditions.

Under the assumption that any practical syngas mixture can be reasonably approximated by a five-component mixture and in the absence of actual data, the method suggests estimating the real syngas $LHV_{s,mix}$ and S_L of the mixture on a molar basis, using Equation (2) and the following Equation (4), respectively:

$$S_L = p[H_2] + q[CH_4] + s[CO] + t[CO_2] + u[N_2] \quad (4)$$

The square brackets in Equation (4) indicate the volume concentration of the species they enclose, whereas the values of coefficients were calculated by a regression analysis of measured data (see [21] for details). Resulting values are: p = 1.2574; q = 0.4605; s = 0.6398; t = −0.2068; u = −0.0284.

Once the $LHV_{s,mix}$ and the S_L of the real syngas are estimated, the composition of the corresponding three-component surrogate mixtures can be derived from the diagram of Figure 2. The diagram is an extended version of the one presented in [21], which relates the couple of values S_L-$LHV_{s,mix}$ of a real syngas mixture to the two parameters α and β of its corresponding surrogate H_2–CH_4–N_2 mixture.

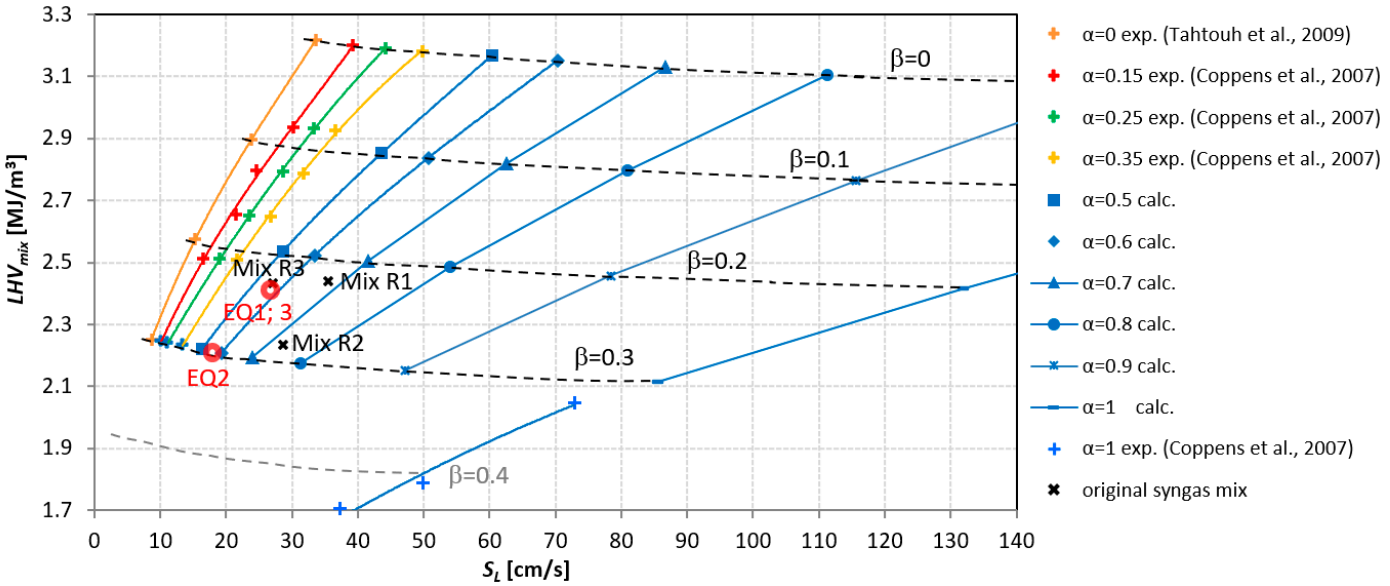

Figure 2. (S_L; LHV_{mix}) surrogate map of the three-component H_2–CH_4–N_2 mixtures obtained via experimental data, and the GRI-Mech 3.0 and San Diego mechanisms. The map is an extended version of the one presented in [21] and includes the experimental data from Tahtouh et al. [22] and Coppens et al. [23].

The first parameter α is defined as the H_2 to H_2–CH_4 volume ratio, whereas β is defined as the ratio between the non-reacting syngas fraction (simulated with a volume of N_2) and the entire fresh charge (i.e., the air volume plus the volume of the non-combustible components). Once the three real syngas components are located in the diagram on the basis of their S_L-$LHV_{s,mix}$ values (see the cross markers in Figure 2), the values of α and β can be determined by graphical interpolation. Then, by the definition of α and β, and by imposing that $[H_2] + [CH_4] + [N_2] = 1$, the composition of the three-component surrogate mixture can be calculated. Note that the value of α for the three fuels MIX R1, MIX R2, MIX R3 spans a rather limited range from approximately 0.56 to 0.72. So, to simplify the management of the experimental campaign, it was decided to only vary the N_2 fraction (i.e., β) to use a unique pressurised tank with $\alpha = 0.6$, i.e., with a volume fraction of H_2 equal to 60% of the entire H_2–CH_4 mixture volume. This leads to S_L values of the surrogate fuels slightly lower than those of the original fuels (except for MIX R3). The two red circle markers in Figure 2 indicated as EQ1;3 (surrogate of MIX R1 and MIX R3) and EQ2 (surrogate of MIX R2) permit a quick estimation of the degree of approximation of the three real fuels. The composition of the H_2–CH_4–N_2 mixtures chosen as surrogates for the three original syngas mixtures is listed in Table 3. Table 3 also includes the composition of the TF and the biogas surrogates (EQTF and EQBG, respectively). In the former, the minimum CO_2 content of the original TF was approximated by a corresponding amount of N_2, whereas in the latter, the minimum H_2 content of the original biogas was simulated with methane, so that EQBG is a simple mixture of pure methane ($\alpha = 0$) and nitrogen ($\beta \approx 0.07$). It is worth noting that the EQTF mixture also shows $\alpha = 0.6$ and so it can be obtained using the same H_2–CH_4 tank selected for the surrogate syngas mixtures.

Table 3. Equivalent mixtures (properties at 15 °C and 1 bar).

Equivalent Fuel	MIX EQ1;3	MIX EQ2	MIX EQBG	MIX EQTF
corresponding real fuel	MIX R1, MIX R3	MIX R2	Biogas	TF
CH_4 [% vol.]	14	11	50	34
H_2 [% vol.]	21	17	0	52
N_2 [% vol.]	65	72	50	14
$[H_2]/([H_2] + [CH_4])$ [%]	60.0	60.0	0	60.0
N_2 [% mass.]	87.0	90.0	64.0	37.0
LHV [MJ/m^3]	6.9	5.5	17.0	16.8
$LHV_{s,mix}$ [MJ/m^3]	2.4	2.2	2.9	3.1
X_a [%]	65	60	83	82

Finally, according to the method presented in [21], the equivalent fuel mixtures so obtained must be checked against the methane number (MN). The MN is defined as the percentage of methane in a methane–hydrogen mixture which has the same resistance to knock as the actual mixture. For example, a fuel with the same anti-knock power as a mixture of 20% hydrogen and 80% methane has a methane number equal to 80. The methane number can be greater than 100 in the case of high concentrations of inert gas in the fuel. There is no a standardized method for the determination of MN. Therefore, different experimental procedures were proposed in the literature [24]. The issue is quite complex as the mixing of some fuels (e.g., CO and CH_4) can lead to much higher flame propagation rates and variable knock resistance (which can be greater or worse) than those of one of the components of the fuel when used alone, under the same operating conditions [25]. Table 4, obtained by processing the data reported in Malenshek et al. [26] and Arunachalam et al. [27], shows MN values measured for different syngas compositions. Comparing these data to those of the syngas mixtures considered here (see Table 3), it descends that the composition closer to all the three mixtures is that obtained from the open top downdraft. Therefore, the MN of the three syngas mixtures would result in the order of 120. However, data of this type do not allow deriving a unique value for a specific blend. Therefore, in the absence of more accurate estimations, MNs can be calculated using the regression model formalised by Equation (5). The model, based on the MN values of known syngas mixtures, provides the following values of the multiplication factors for each species concentration: $a = -0.012$, $b = 1.0055$, $c = 0.1779$, $d = 1.977$, and $e = 0.9973$ (see [21] for details).

$$MN = a[H_2] + b[CH_4] + c[CO] + d[CO_2] + e[N_2] \quad (5)$$

Table 4. Methane number of different synthesis gases adapted from Malenshek et al. [26] and Arunachalam et al. [27].

Test Gas	Ref.	H_2 [%vol.]	CH_4 [%vol.]	CO [%vol.]	CO_2 [%vol.]	N_2 [%vol.]	MN
Reformed natural gas	[26]	37.9	19.5	8.1	9.3	25.2	61.8
Coal gas	[26]	33.3	3.2	53.1	3.7	6.7	26.9
Wood gas	[26]	31.1	1.5	17.5	16.2	33.7	69.9
Digester gas	[26]	0.0	60.3	0.0	37.9	1.8	139.1
Landfill gas	[26]	0.0	60.4	0.0	39.6	0.0	139.6
Fluidized bed	[27]	38.6	10.3	23.8	22.5	4.8	55.6
Two stage gasification	[27]	29.6	2.6	17.7	14.9	35.2	54.6
Updraft	[27]	20.5	6.0	22.7	12.7	38.1	105.6
Downdraft	[27]	20.1	3.0	21.3	2.0	53.6	57.5
Open top downdraft	[27]	19.7	2.1	19.3	12.9	46.0	125.7

Equation (5) gives the MN estimations listed in Table 5. The table shows that the MN of the syngas surrogate fuels are not far from (slightly higher than) the corresponding MN of the original fuels. Thus, the test with the syngas surrogates should lead to a reliable

prediction of the optimum spark advance (SA), even if in an SA lower than the optimum value obtained from the test could be necessary during real gas operation in case the tests indicate an optimum SA close to borderline knock.

Table 5. Methane number of the three syngas mixtures (MIX R1, MIX R2, MIX R3) and two surrogates fuels (MIX EQ1;3, MIX EQ2) as estimated using Equation (5).

Syngas	MN	Surrogate	MN
MIX R1	73.3	MIX EQ1;3	78.7
MIX R2	80.7	MIX EQ2	82.7
MIX R3	85.3	MIX EQ1;3	78.7

On the other hand, Figure 2 shows that the S_L of the syngas surrogates are generally lower than those of the corresponding original fuels. Accordingly, a slightly higher fuel conversion efficiency η_f is expected from operation with the original syngas fuels. Thus, the specific fuel consumption of the engine during operation with the original syngas fuels should be slightly lower than the specific fuel consumption measured during the present experiments.

4. Experimental Setup

According to the arguments presented in Section 2, two different lines were set up for fuelling the engine: one for the combustible part of the equivalent mixtures (i.e., a blend of CH_4 and H_2) and one for the inert part (i.e., a stream of N_2). The two lines are shown in Figure 3a,b, respectively. Three pipes, whose total section is approximately half that of the air manifold, were added to introduce N_2 upstream of the air compressor, so that the air entering the engine changes according to the amount of N_2 injected (the three ducts are highlighted by three dashed lines in Figure 3b). A Coriolis mass flow meter with a range of 50 kg/h was installed on the CH_4–H_2 mixture line, while a mass flow meter with a full scale of 120 kg/h was installed on the inert line. A multi-stage pressure reducer system was developed to control the N_2 flow rate. The system includes the same kind of pressure reducers installed on commonly natural gas engine vehicles, modified to be controlled through a vacuum signal generated by the airflow crossing a suitably sized Venturi. Three reducers in parallel were necessary to reach an N_2 flow rate of approximately 120 kg/h.

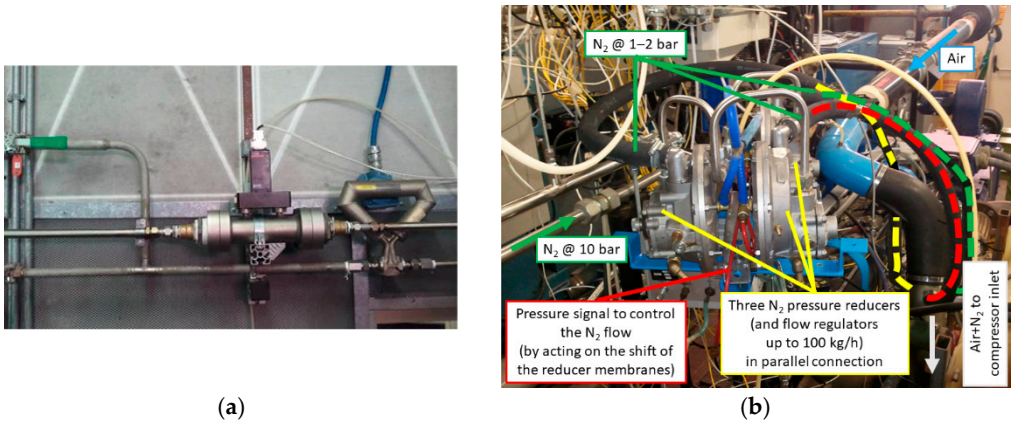

(**a**) (**b**)

Figure 3. Lines and mass flow meters for equivalent syngas fuelling: (**a**) combustible fraction (CH_4 and H_2); (**b**) inert fraction (N_2). Nitrogen is delivered by tanks at 10 bars.

To make a tested mixture equivalent to the reference mixture, the ratio between the mass flow rates of the combustible fraction and the inert was checked online, setting it equal to that of Table 3 in accordance with Equation (6).

$$N_2\%mass = \frac{N_2 mass}{N_2 mass + (N_2 - CH_4)mass} \quad (6)$$

The experimental setup and the adopted method allowed a good accuracy in setting the nitrogen percentage as the flow rate of the combustible fraction varies. Figure 4 shows some measurements acquired during a preliminary checking of the fuel control system. Data are related to MIX EQ2, a mixture with a mass percentage of N_2 equal to 90%. It clearly appears that only few measurements must be discarded to maintain the accuracy of approximately ±0.5% in the achievement of the target value of N_2 mass fraction.

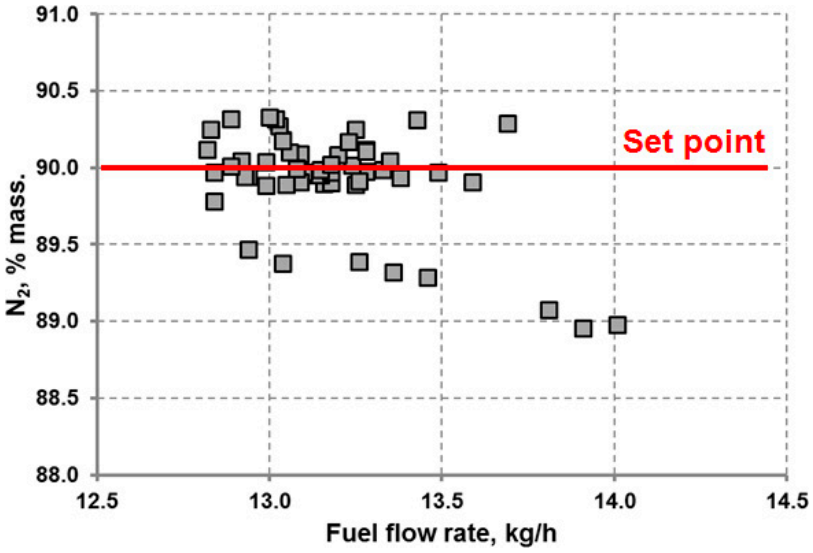

Figure 4. Distribution of the actual mass percentage of nitrogen, with respect to the set point, as a function of the fuel flow rate.

The main characteristics of the engine used for the experimental activity are shown in Table 6 where the maximum performance refers to the CNG operation. The engine was connected to a dynamic bench equipped with an asynchronous electric machine (315 kW from 2000 to 3500 rpm) suited to bus engine testing. Tests were carried out in conditions resembling those of stationary power plants for the production of electricity with syngas engines: stoichiometric power supply, speed of 1500 rpm, and 1250 mbar of absolute pressure in the intake manifold (MAP). Therefore, concerning the maximum performance of the engine powered by CNG (Table 6), lower torque values were reached, in the range of 400 ÷ 600 Nm, both for the lower boost pressure and for the lower $LHV_{s,mix}$.

Table 6. Main characteristics of the engine used in the tests when fuelled with CNG.

Characteristic	
Engine type	SI, turbocharged
Number of cylinders	6
Bore × stroke, mm	115 × 125
Compression ratio	11:1
Ignition system	one coil per cylinder
Maximum power (CNG)	200 kW@2100 rpm
MAP at max. power (CNG)	1.5 bar

A KISTLER® piezoelectric pressure transducer (sensitivity 26 pC/bar) was installed in the combustion chamber of cylinder no. 1 of the engine for the acquisition of the pressure cycle with an Indicom AVL® system. The pressure signal of 70 consecutive cycles was processed online to derive the heat release rate useful for describing the combustion behaviour and the other cycle parameters. The instrumentation listed in Table 7 was used to measure engine performance and emissions.

Table 7. Main characteristics of the test equipment.

Measurement	Instrument	Full Scale Reading	Accuracy
Torque	HBM® T 10F torque flange	±0–2000 Nm	±0.2% full scale
Rotational speed	Heidenhain® encoder	0–3500 rpm	±1 rpm
Brake power	AFA AVL DINAMOMETER	−280–315 kW	±0.2% full scale
Fuel mass flow rate	Coriolis MICRO MOTION ELITE	0–50 kg/h	<1% full scale
N_2 mass flow rate	BROOKS thermal mass flow meter	0–120 kg/h	<2% full scale
Air mass flow rate	ABB SENSY FLOW P mass flow meter	0–1200 kg/h	±1% full scale
THC conc.	ABB MULTIFID 14 EGA	0–10,000 ppm C_3	0.5% full scale
NO_X conc.	CLD ECOPHYSICS	0–5000 ppm	<1% full scale
CO_2 conc.	ABB URAS 14 EGA	0–20%	1% full scale
O_2 conc.	ABB MACROS 16 EGA	0–25%	0.5% full scale

5. Ignition System

The original ignition system was replaced with a non-conventional one, which is capable to control the energy of the ignition by modifying the duration and the intensity of the electric discharge. The system was interfaced with the engine phase sensor to set the proper ignition timing. Spark plugs with a gap of 0.25 mm were initially used. The coil signal was acquired with a Hall effect current sensor (maximum current 55 A), installed on the positive lead of the coil primary power circuit. The current sensor allows the characterization of the ignition system as follows.

Figure 5 refers to engine operation with MIX EQ2 and reports on the left-side ordinates the value of the current in the primary circuit coil as a function of the crank angle. The corresponding value of the voltage induced on the secondary circuit (V_S) can be read on the right-side ordinates for two ignition conditions (see the red and blue curves in the figure named in the legend as 32 mA/300 μs and 32 mA/800 μs, respectively). During the excitation phase, the ignition system provides a step-like increase of the primary current up to a peak value I_{P1} approximately equal in the two ignition conditions. The corresponding voltage induced in the secondary coil circuit suddenly increases up to approximately 3 kV (V_{S1}) originating the spark at the plug electrodes. Note that such a type of ignition system operates very differently from a conventional one. The latter obtains the spark when the primary current is sharply interrupted and the corresponding sudden variation of the magnetic flux, according to the Faraday's law, induces the secondary voltage spike necessary to start the breakdown phase. Instead, the ignition system under analysis, builds up the primary current just for the induction of the high secondary voltage which causes the breakdown, and keeps the primary current on during the spark discharge to achieve a target spark duration and intensity. In fact, in the two ignition configurations considered here, the primary current was built-up at the same time instant (i.e., same spark timing equal to 32 crank angle degree—CAD—before top dead centre—BTDC) to the same level I_{P1}, to obtain the same level of the secondary circuit current (32 mA). By properly modulating these parameters, the spark is sustained for very different time durations (i.e., spark durations), equal to 330 and 800 μs, respectively.

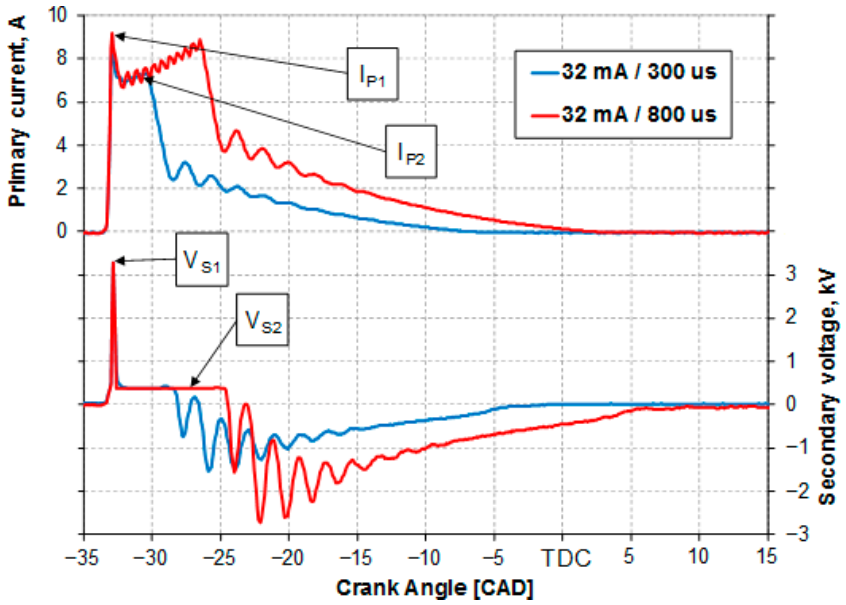

Figure 5. Primary coil circuit current and secondary coil circuit voltage, for two different spark duration conditions (300 and 800 µs) with the same target current intensity on the secondary (32 mA) with MIX EQ2.

In detail, after the rapid increase up to I_{P1}, the primary current was rapidly reduced and then increased again, but to a much lower growth rate than the initial phase. During this second phase, the so-called "holding current" I_{P2} is characterized by small oscillations and variable duration, the value of which depends on the control parameters of the ignition system. The holding current increases the spark energy and causes a residual secondary V_{S2} voltage on the secondary circuit. Looking at the secondary coil circuit voltage curve, the peak V_{S1}, which triggers the spark ignition, is followed by a few crank-angle degrees interval in which the voltage is kept at a much lower value V_{S2}. This voltage, approximately equal to 300 V, is suitable to maintain the charging current I_{P2} in the primary circuit. After this, the primary coil current quickly halves, indicating that the energizing of the ignition circuit was switched off. This induces high-voltage variations on the secondary coil circuit, as in a conventional ignition system, so that other sparks are released from the spark plug. This is the second spark phase of such an ignition system type. In fact, the secondary voltage fluctuations, before gradually cancelling out each other, measure a few thousand volts. The second spark phase is generally irrelevant in the optimal ignition conditions, i.e., when the ignition and the propagation of combustion take place efficiently. In this condition, the sparks generated in the second phase do not contribute to the combustion since the flame front has already moved away from the spark plug electrodes after the initial spark caused by the peak current I_{P1}. On the other hand, the second spark phase could be beneficial in more critical conditions when combustion and flame propagation are difficult to trigger and sustain, respectively (for example, when using combustible mixtures highly diluted with inert species). In these circumstances, the additional energy supplied during the second phase of the ignition process can strengthen the initial flame kernel and increase the chances of effective ignition and flame propagation. Due to the specific characteristics of the coils, the system can vary the ignition energy in the range from 80 to 300 mJ, by changing the duration and intensity of the primary circuit-charging current. The values of the two pair of parameters can be set arbitrarily within the range shown in Figure 6. Therefore, it is not possible to combine the longer durations with the higher spark intensities due to the 300 mJ limit, which corresponds to the upper right bound in Figure 6.

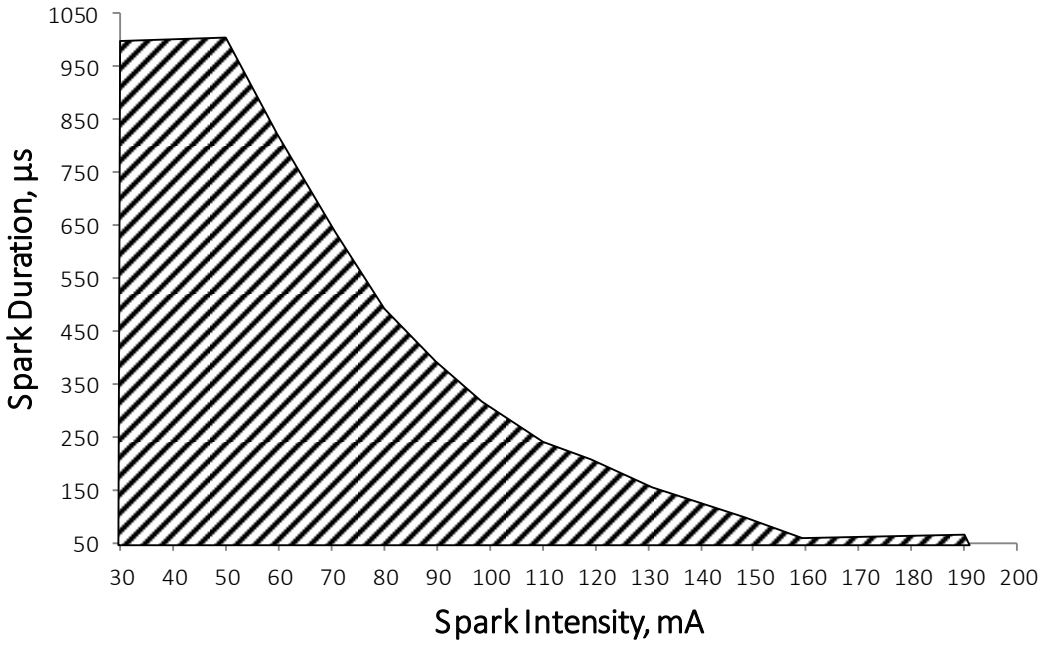

Figure 6. Target values of secondary coil-circuit current intensity and duration of the spark achievable by the ignition system.

6. Results

6.1. Maximum Load

High load tests were performed at 1250 mbar of MAP and 1500 rpm. In such conditions, the effects of the ignition parameters on the engine performance are not very relevant. Figure 7 shows the current intensity in the primary circuit and the heat release as a function of the crank angle when the engine is fuelled with MIX EQ2.

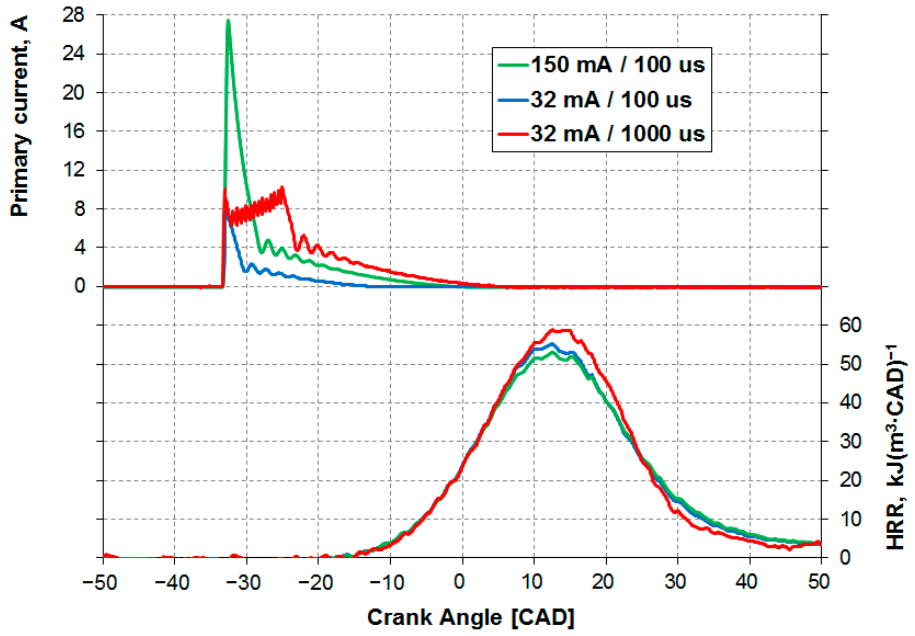

Figure 7. Heat release rate and primary coil current, for different ignition conditions, with MIX EQ2 at 1500 rpm and MAP 1250 mbar.

This is the most challenging of the fuel mixtures considered in the present work because MIX EQ2 shows the highest percentage of N_2 and so it is particularly difficult to ignite. In Figure 7, the test conditions differ in the duration and intensity of the ignition

phase. A slight but appreciable difference between the two heat release rate curves occurs only when the discharge duration is increased up to 900 µs (corresponding to approximately 8 CAD at 1500 rpm). In detail, the curve recorded with the longer discharge duration (1000 µs, 9 CAD) shows a higher heat release peak and faster completion of the rapid combustion phase. On the contrary, an increase in the current intensity does not lead to higher combustion speed if a stable start of combustion is already possible with lower current values. Thus, the longer energization duration turns out to be slightly more effective than the greater peak intensity in improving combustion.

Only two tests for each target duration of the set discharge were therefore performed to study the high-load engine operations with different fuels: one with minimum energy and one with maximum energy. Independently on the fuel mixture, the SA was set to obtain 50% of the fuel burnt mass at approximately 10 CAD after the top dead centre (TDC) for all the tests. This allows the study of the effects of ignition parameters at SAs close to the optimal values (i.e., close to maximum brake torque, MBT).

In the series of graphs which follows, the ignition conditions are discriminated based on energy alone regardless of the duration and target intensity of the spark. Accordingly, at the same value of ignition energy on the abscissa, the test points refer to different duration/intensity settings. Furthermore, each test point was repeated three times to evaluate the dispersion of the measurements, represented in the graphs with error bars. The minimum and maximum energy conditions were tested with more intensity–duration combinations than the intermediate values, obtaining a greater dispersion of the results.

Figure 8a shows the brake-specific fuel consumption (BSFC) of the engine, measured during operation with the four fuel surrogates for different ignition energies.

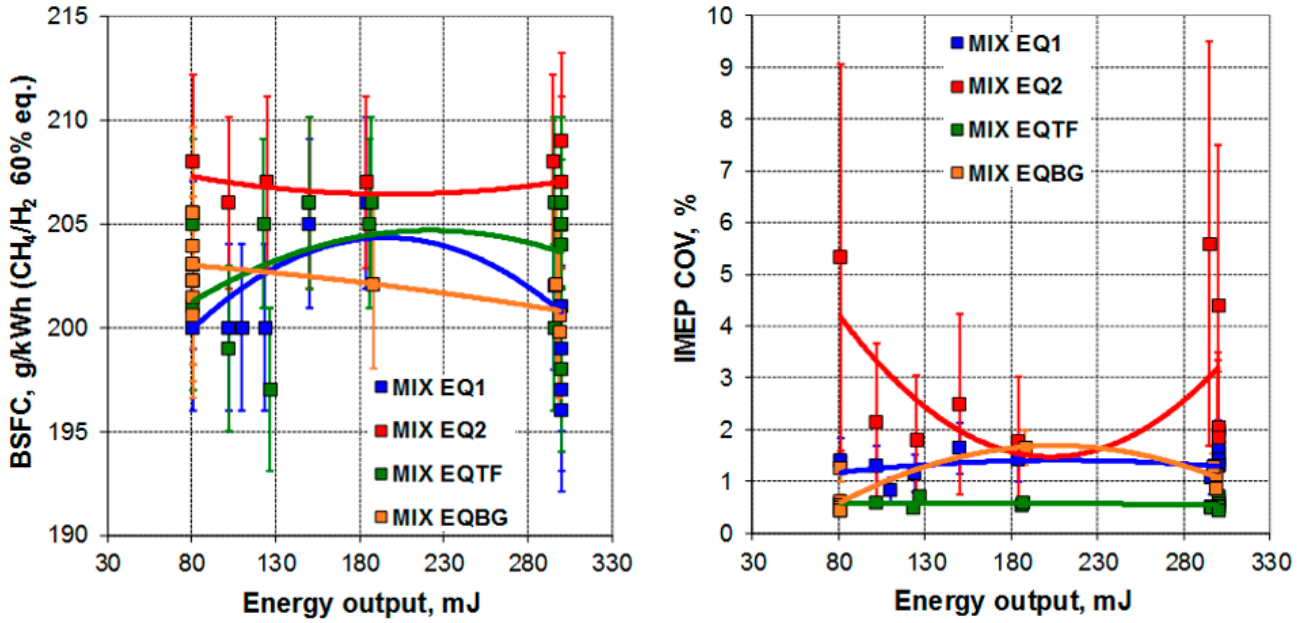

(**a**) (**b**)

Figure 8. Different ignition condition data for operation with the equivalent mixtures at 1500 rpm and MAP 1250 mbar: (**a**) BSFC considering only the mass of CH_4–H_2; (**b**) IMEP COV.

The BSFC does not vary appreciably, independently of the way in which the ignition energy is increased (i.e., by either acting on the duration of the discharge, or on the current intensity or both), even if the extreme values of data scattering are considered. The BSFC data are defined based on the sole combustible part of the syngas to make the comparison between operations with very different syngas fuels possible. Therefore, BSFCs were obtained directly from the measurement of the fuel mass flow rate (for MIX EQ1;3, EQ2 e EQTF) and the shaft power without taking into account the nitrogen flow

rate. For MIX EQBG case, the equivalent BSFC was obtained by multiplying the measured methane flow rate by the calorific value of the methane and dividing by the calorific value of the mixture CH_4–H_2 at 60% by volume of H_2. Despite the low differences in the dataset, there is a slightly greater BSFC for MIX EQ2 blend (90% nitrogen volume fraction), compared to MIX EQ1;3, EQBG, and EQTF blends. As the inert content increases, conditions for the completion of combustion become more critical. This fact is supported by Figure 8b, which reports the coefficient of variation (COV) of the indicated effective mean pressure (IMEP). Data related to MIX EQ2 show a considerable dispersion due to the acquisition of some cycles characterized by partial ignition phenomena. On the contrary, more stable combustion was observed for MIX EQ1;3, EQBG, and EQTF surrogate fuels, all characterised by values of IMEP COV lower than 3%.

Combustion instability directly affects total unburned hydrocarbon (THC) emissions measured at the exhaust, as shown in Figure 9a. Figure 9b shows the NO_x emissions data. These values are not affected by the setup of ignition parameters, whereas they noticeably reduce as the concentration of inerts increases, i.e., moving from MIX EQTF to MIX EQBG to MIX EQ1;3 up to MIX EQ 2. In fact, the level of NO_x emission strongly depends on the maximum combustion temperature and, at constant 50% burnt mass for each surrogate fuel operation, the higher the amounts of inert species, the lower the temperature peaks in the combustion chamber. Combustion instability occurring during EQ2 operation should contribute to a reduction in exhaust NO_x as well. However, since NO_x are already very low for MIX EQ2 operation, this effect is not appreciable from the measurements.

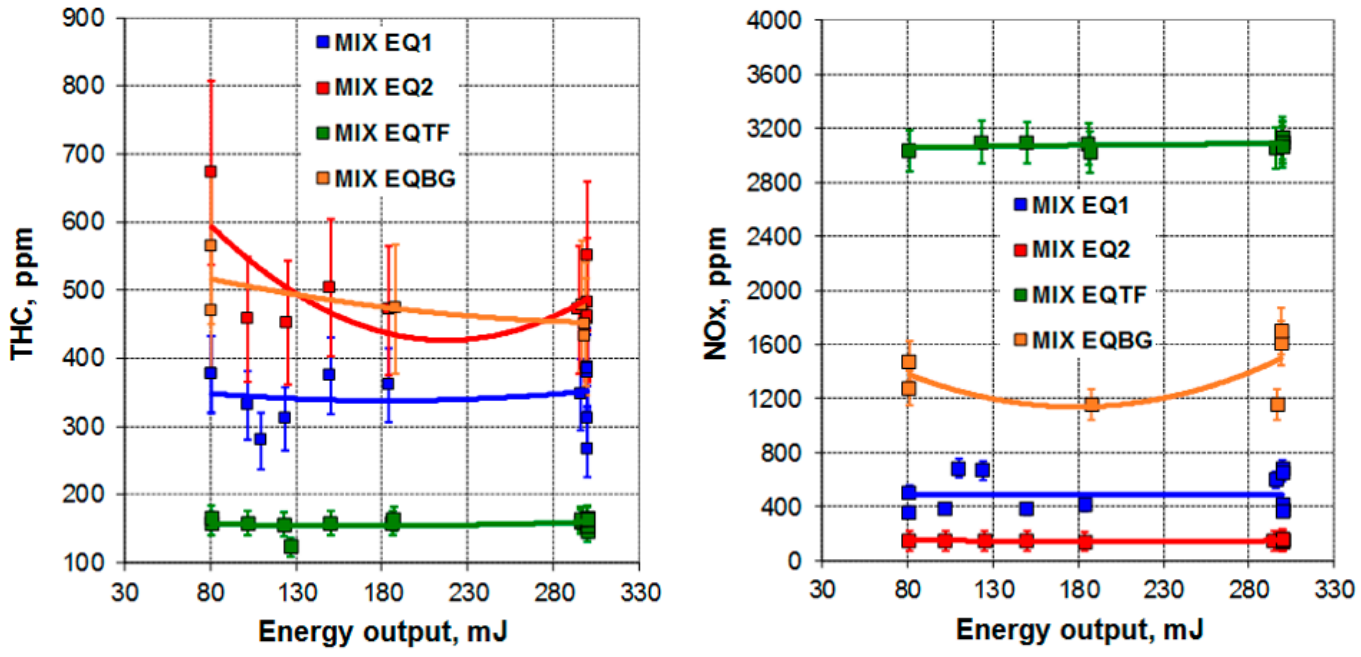

(**a**) (**b**)

Figure 9. Measured emissions as a function of the ignition energy for operation with the equivalent mixtures at 1500 rpm and MAP 1250 mbar: (**a**) THC; (**b**) NOx.

Results obtained from the high-load tests suggest that engine operations at the same reliability levels as those measured here could be obtained even with an ignition energy lower than the minimum allowed by the available ignition system. It is clear that, below a certain energy ignition, the performance of the engine should deteriorate. Thus, all the tests performed to find the optimum SA for each fuel under investigation as well as the sensitivity of the engine performance to the SA, were carried out at 80 mJ of ignition energy, the minimum energy admitted by the ignition system. In the following graphs, in which a single pair of intensity–duration parameters was tested, the error bars represent the

variability of the measurement during acquisition time, while the point is the average value. Figure 10a shows the BSFC sensitivity to the SA as measured for the engine operation with the four surrogate fuels. In terms of BSFC, MIX EQTF results the fuel less sensitive to SA, the syngas surrogates show approximately the same sensitivity, whereas the data collected for MIX EQBG do not allow for the comparison because they span a CAD range centred around an excessively high SA. The optimum SA increases as the content of inert gasses in the fuel increases: inert gasses hinder the progress of combustion and slow down its progression. In particular, the optimum SA is approximately equal to 12 CAD for MIX EQTF, 15 CAD for MIX EQBG, 28 CAD for MIX EQ2, and 36 CAD for MIX EQ1;3. However, it is necessary to verify that such optimal SAs can be effectively set, without the risk of abnormal combustions, which can compromise the engine integrity. To this end, an evaluation of the combustion trend was carried out based on the maximum peak of the pressure gradient in the combustion chamber. This parameter is an alert for possible knocking combustion when it approaches the limit value of approximately 10–15 bar/CAD. Figure 10b shows that the optimum SA values lead to a maximum peak of the pressure gradient equal to—or higher than—10–15 bar/CAD only in the case of MIX EQTF. Although reaching this conventional limit does not automatically mean that borderline knock operations are achieved (especially when deflagration combustion with a high flame-speed mixture is concerned), it is anyway safe to introduce some delay in the SA to limit the mechanical loads of an engine design originally conceived for operations with smaller pressure gradients.

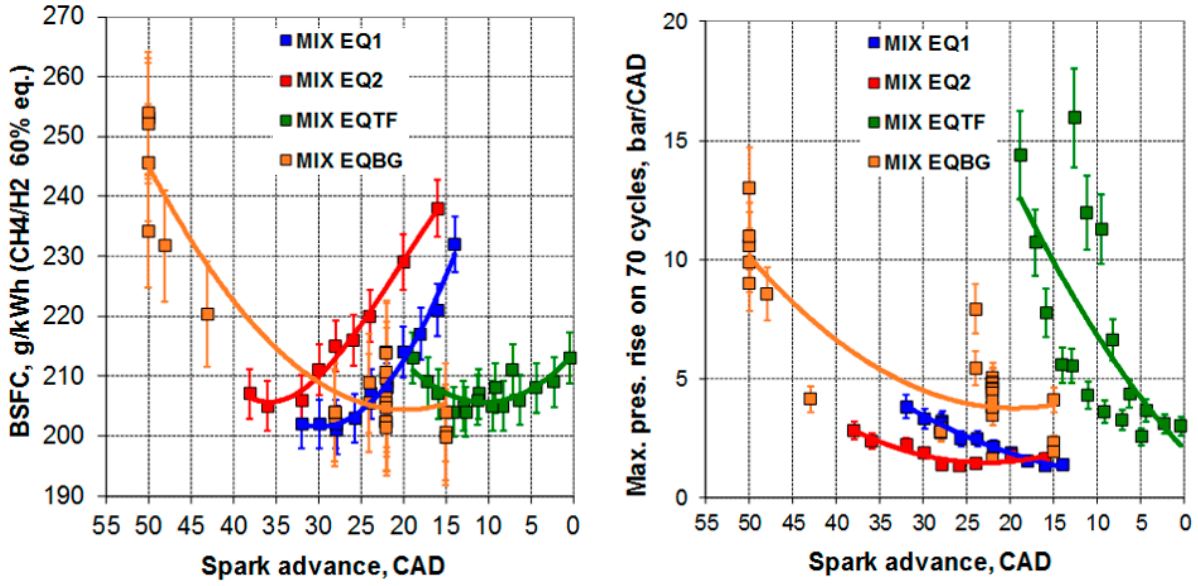

(**a**) (**b**)

Figure 10. Different SA data for minimum ignition energy operation with the equivalent mixtures at 1500 rpm and MAP 1250 mbar: (**a**) BSFC; (**b**) maximum pressure rise over 70 consecutive cycles.

On the other hand, the syngas surrogate mixture with a higher inert content (MIX EQ2), which does not seem to exhibit operation issues from Figure 10, originates a large number of cycles with partial combustion as the SA is increased, as highlighted by the trends of THC emissions reported in Figure 11. When the engine is fuelled with MIX EQ2, THC emissions grow more rapidly than with the other fuel mixtures, index of a greater effect than that expected for the trapping of the fuel in crevices.

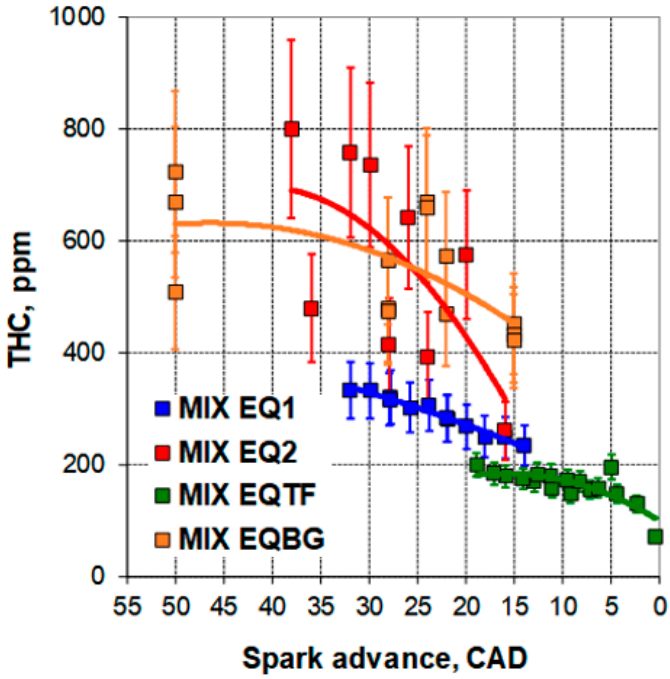

Figure 11. THC data for different SAs operation with minimum ignition energy at 1500 rpm and MAP 1250 mbar.

This aspect could represent a limit to the optimization of syngas engines because high SAs needed to compensate for the reduced combustion speed can cause irregular engine operation. However, this behaviour was not detected for the other syngas surrogate mixture (i.e., MIX EQ1;3) despite its considerable content of N_2.

6.2. Critical Ignition Conditions

The engine equipped with the non-conventional ignition system did not show any particular operating problem at maximum load, apart from the occurrence of partial combustion found for high SA values when the engine is fuelled with MIX EQ2. Nevertheless, it is expected that excessively low values of the ignition energy could compromise the engine operation. Therefore, in order to analyse the ignition phase in more detail, further tests were carried out aimed at reaching critical conditions. To this end, the biogas surrogate MIX EQBG, showing the average highest THC emissions in the SA range considered in Figure 11, was assumed as starting point for further experiments. It was modified introducing different degrees of dilution with nitrogen, from 0 to 90% by mass, varying the engine load, and the SA. In order to retain stoichiometric fuelling, the engine load and MAP were reduced contextually. In particular, the MAP was varied in the range 820–1330 mbar, while the SA was increased starting from minimum values, corresponding to delayed combustion, up to the maximum possible value admitted. Spark advance is limited by either the control system (50 CAD BTDC), or by the achievement of highly unstable conditions, characterized by a COV of the IMEP greater than 10%. It should be noted that the value of the SA limit, beyond which the COV exceeds 10%, is affected by some inaccuracy due to the very irregular engine operation. Each engine operating point considered was tested setting the ignition system to the minimum (80 mJ) and the maximum (300 mJ) ignition energy output. Figure 12 shows the curves of the misfire limit obtained by setting the SA at different dilution of the combustible with N_2. Tests were performed at three MAP values, and at minimum and maximum ignition energy.

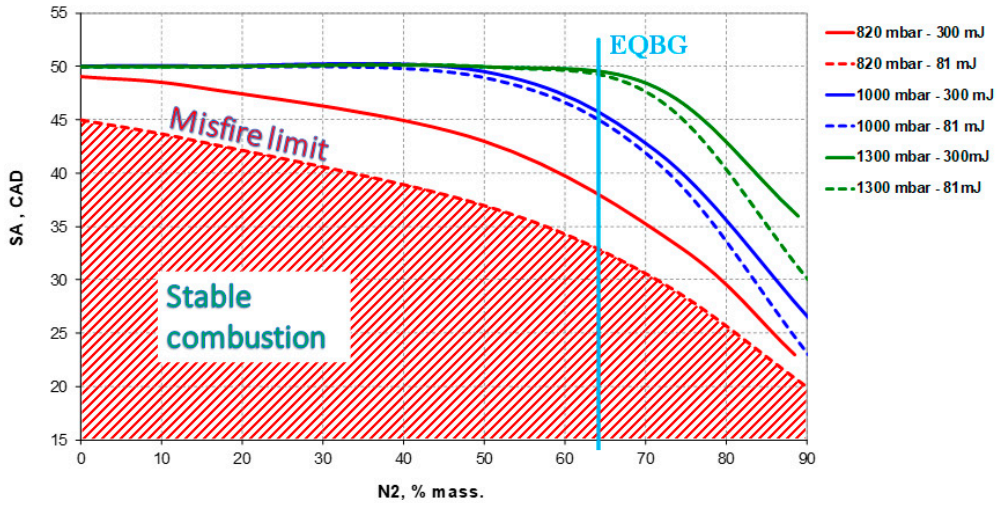

Figure 12. SA limit for combustion stability of CH_4 as a function of the N_2 mass fraction dilution.

Measured values demonstrate that the misfire-limited SA angle decreases as the dilution increases. The constraint imposed by the misfire occurrence on the maximum achievable SA dominates the low-load operation, regardless of the fuel dilution. Instead, the mentioned constraint is stronger than the SA limit admitted by the ignition system only for fuel dilution higher than 50–60% by mass at high loads. The most critical conditions tested were those with the lowest MAP (820 mbar). In these conditions,an increase of the ignition energy from 80 to 300 mJ allows for more regular engine operation at each degree of fuel dilution, as demonstrated by the higher value of the maximum-tolerated ignition advance before the misfire occurrence. The MAP increase, which also increases the cylinder pressure, promotes the stability of engine operation. At MAP equal to 1000 and 1300 mbar, with dilutions lower than 50–60%, the SA limit could exceed the maximum one admitted by the control system, still maintaining regular combustion. For over 60% dilution, the advantage associated with the increase of the ignition energy in terms of maximum SA before misfire occurrence is apparent at any engine load.

The results described can be explained by focusing on the conditions of the combustible mixture present between the spark plug electrodes. It is clear that as the MAP decreases (i.e., the engine load decreases), the mass density of the air–fuel mixture in the cylinder decreases as well. Accordingly, the lower the MAP, the higher the rarefaction of the fresh charge at the end of the compression phase, i.e., exactly at the beginning of the spark. Consequently, the energy released by the mixture combustion close to the spark plug electrodes decreases. This energy becomes even smaller if the SA is increased; in fact, the greater the SA, the greater the cylinder volume occupied by the mixture and the lower the mass density at the time of spark. As the dilution of the inert gasses contained in the syngas increases, part of the mixture near the spark plug electrodes not only does not contribute to the energy release during combustion but also lowers the temperature of the reaction. Ultimately, the reduction of the load, associated with high values of SA and inert dilution, causes the spark to take place when the pressure and temperature in the combustion chamber make the propagation of the flame front difficult. This is due to the small energy released at the start of ignition and the corresponding small kernel of flame. To verify this hypothesis, tests were carried out with a gap between the electrodes of the spark plugs, which increased from 0.25 to 0.5 mm, to increase the amount of mixture between the spark plug electrodes. The tests were conducted by reducing the MAP up to 300 mbar, to explore conditions that are even more critical, feeding the engine with MIX EQ2, and setting the ignition energy at a maximum value of 300 mJ.

The results, shown in Figure 13, demonstrate that a 0.50 mm gap between the spark plug electrodes permits to decrease the minimum load for stable engine operation, while maintaining low THC emissions. In fact, engine operation becomes unstable only at very

low loads (MAP below 400 mbar) and remains very stable at low-to-medium load. With a 0.25 mm spark plug gap, cycles characterised by partial combustion and high THC emissions already occurred in operation at MAP just below 700 mbar.

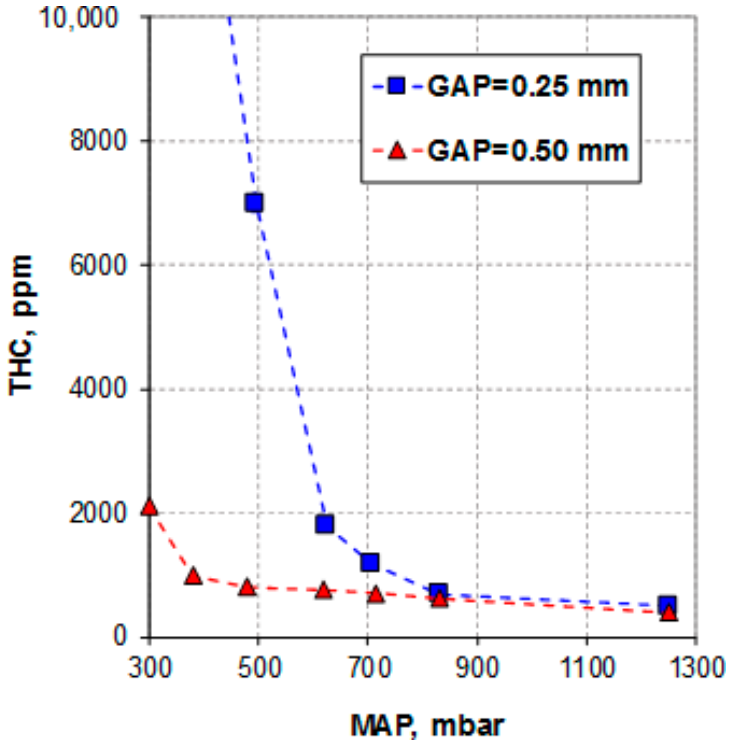

Figure 13. Effect of the spark plug gap on THC emissions as a function of MAP (data recorded at 1500 rpm, SA 23 CAD and ignition energy 300 mJ).

7. Conclusions

A study was carried out on the behaviour of an internal combustion engine when powered with ternary gas mixtures composed by methane, hydrogen, and nitrogen. Mixture compositions were defined to simulate different types of syngas as well as a biogas and a hydrogen–methane mixture with EGR, all approximating possible fuel mixtures for the transition towards a 100% renewable energy system. In particular, fuel mixtures with calorific values in the range 5–22 MJ/Nm^3 were considered. The experimental study investigated the engine performance and identified the optimal setup parameters of a non-conventional ignition system that was selected to extend the stable operation limits of a natural gas engine modified to be fuelled with low-quality gaseous fuel mixtures.

None of the considered fuel mixtures justifies the increase of the ignition energy beyond 80 mJ (the minimum energy level investigated). The spark advance for minimum brake-specific fuel consumption has been experimentally obtained during engine operation at maximum load with a pressure in the intake manifold equal to 1250 mbar. It was demonstrated that optimum spark advance operations are possible at full load for all the fuels with exception of the syngas with lower LHV, where partial combustion phenomena impose a higher than optimum spark advance. Only the pure methane–hydrogen fuel with a 3.5% EGR requires a spark advance slightly lower than the optimum one to contain the maximum pressure gradients within acceptable limits for the reliability of engine operation. The results at full load operation with optimised spark advance indicate substantial independence of the engine performance from the ignition system parameters for all the fuel mixtures considered in this work. Nevertheless, it has been observed that, as the inert content increases, the operation of the engine becomes irregular not only at reduced spark advances, as it is expected because of the slowing effect of the combustion speed, but also at high spark advances. The maximum spark advance for which the combustion

becomes highly irregular decreases with inert content but also at reduced engine loads. This behaviour is due to the increased dilution with inert species of the fresh charge between the spark plug electrodes at the time of ignition. Such dilution reduces the size of the initial flame kernel, especially at higher values of the spark advance, where the rarefaction of the in-cylinder charge is higher. Thus, during critical ignition operation of the engine, the increase of the ignition energy, obtained through the greater energization of the primary circuit, leads to an increase of the maximum ignition advance tolerated. In fact, with more ignition energy, the non-conventional ignition system allows for high intensity of the sparks, which increases the flame kernel size, and multiple spark repetitions, which means the reaching of a larger portion of the mixture in motion close to the electrodes. Both these system features contribute to widen the stable operation range of the engine up to very low loads even with the lower LHV syngas.

The ignition parameters and the spark plug features also affect the power absorbed by the ignition system and the long-term durability of the engine. Consequently, the results of this work can give useful information to optimise the design of new ignition systems as a function of the type of non-fossil fuel chosen for the operation of either an existing or a new engine design.

Author Contributions: Conceptualization, L.D.S., S.I. and M.M.; methodology, L.D.S., S.I., P.G. and M.M.; software, P.G.; validation, L.D.S. and S.I.; formal analysis, L.D.S. and S.I.; investigation, L.D.S. and S.I.; resources, L.D.S. and S.I.; data curation, L.D.S. and S.I.; writing—original draft preparation, L.D.S., S.I., M.M. and P.G.; writing—review and editing, L.D.S., S.I., P.G. and M.M.; visualization, L.D.S., S.I. and M.M.; supervision, L.D.S., S.I. and M.M.; project administration, L.D.S. and S.I.; funding acquisition, L.D.S. and S.I. All authors have read and agreed to the published version of the manuscript.

Funding: This research was funded by a research contract with Engine Technology Solutions, a private company operating in the energy sector.

Data Availability Statement: Not applicable.

Acknowledgments: The authors are grateful to Vicenzo Bonanno for his valuable support in the experimental activities.

Conflicts of Interest: The authors declare no conflict of interest.

References

1. Danieli, P.; Lazzaretto, A.; Al-Zaili, J.; Sayma, A.I.; Masi, M.; Carraro, G. The potential of the natural gas grid to accommodate hydrogen as an energy vector in transition towards a fully renewable energy system. *Appl. Energy* **2022**, *313*, 118843. [CrossRef]
2. Publications Office of the European Union. *Hydrogen Roadmap Europe: A Sustainable Pathway for the European Energy Transition*; Publications Office: Luxembourg, 2019. Available online: https://data.europa.eu/doi/10.2843/341510 (accessed on 25 October 2022).
3. Gobbato, P.; Masi, M.; Benetti, M. Performance analysis of a producer gas-fuelled heavy-duty SI engine at full-load operation. *Energy Procedia* **2015**, *82*, 149–155. [CrossRef]
4. Bridgwater, A.V. The technical and economic feasibility of biomass gasification for power generation. *Fuel* **1995**, *74*, 631–653. [CrossRef]
5. Chapman, K.S.; Patil, A. *Performance, Efficiency, and Emissions Characterization of Reciprocating Internal Combustion Engines Fuelled with Hydrogen/Natural Gas Blends*; Technical Report DOE Award DE-FC26-04NT42234; Kansas State University: Manhattan, KS, USA, 2008. [CrossRef]
6. Boulouchos, K.; Dimopoulos, P.; Hotz, R.; Rechsteiner, C.; Soltic, P. Combustion Characteristics of Hydrogen-Natural Gas Mixtures in Passenger Car Engines. In Proceedings of the 8th International Conference on Engines for Automobiles (ICE 2007), Capri, Italy, 16–21 September 2007; pp. 1–15, SAE Technical Paper No. 2007-24-0065. [CrossRef]
7. Tunestål, P.; Christensen, M.; Einewall, P.; Andersson, T.; Johansson, B.; Jönsson, O. Hydrogen Addition for Improved Lean Burn Capability of Slow and Fast Burning Natural Gas Combustion Chambers. In Proceedings of the SAE Powertrain and Fluid Systems Conference and Exhibition, San Diego, CA, USA, 21–24 October 2002; pp. 1–13, SAE Technical Paper 2002-01-2686. [CrossRef]
8. Bysveen, M. Engine characteristics of emissions and performance using mixtures of natural gas and hydrogen. *Energy* **2007**, *32*, 482–489. [CrossRef]

9. Teoh, Y.H.; Masjuki, H.; Kalama, M.; Howa, H.G. Effect of injection timing and EGR on engine-out-responses of a common-rail diesel engine fueled with neat biodiesel. *RSC Adv.* **2015**, *5*, 96080. [CrossRef]
10. De Simio, L.; Gambino, M.; Iannaccone, S. Effects of EGR on Engines Fueled with Natural Gas and Natural Gas/Hydrogen Blends. In *Natural Gas Engines. Energy, Environment, and Sustainability*; Srinivasan, K., Agarwal, A., Krishnan, S., Mulone, V., Eds.; Springer: Singapore, 2019. [CrossRef]
11. Costa, M.; Prati, M.V.; De Simio, L.; Iannaccone, S.; Piazzullo, D. CFD study of a CI engine powered in the dual-fuel mode with syngas and waste vegetable oil. *J. Phys. Conf. Ser.* **2021**, *1868*, 012014. [CrossRef]
12. Gamiño, B.; Aguillón, J. Numerical simulation of syngas combustion with a multi-spark ignition system in a diesel engine adapted to work at the Otto cycle. *Fuel* **2010**, *89*, 581–591. [CrossRef]
13. Jang, J.H.; Huang, D.Y.; Lin, P.H.; Chen, B.H. Effect of Ignition Timing on the Emission of Internal Combustion Engine with Syngas Containing Hydrogen using a Spark Plug Reformer System. *Energy Procedia* **2017**, *105*, 1570–1575. [CrossRef]
14. Wang, C.H.; Kan, X.; Zhou, D.; Yang, W.; Zhai, X. An investigation on utilization of biogas and syngas produced from biomass waste in premixed spark ignition engine. *Appl. Energy* **2018**, *212*, 210–222. [CrossRef]
15. Hagos, F.Y.; Aziz, A.R.A.; Sulaiman, S.A. Trends of syngas as a fuel in internal combustion engines. *Adv. Mech. Eng.* **2014**, *6*, 1–10. [CrossRef]
16. Fiore, M.; Magi, V.; Viggiano, A. Internal combustion engines powered by syngas: A review. *Appl. Energy* **2020**, *276*, 115415. [CrossRef]
17. Heywood, J.B. *Internal Combustion Engine Fundamentals*, 2nd ed.; McGraw-Hill Education: New York, NY, USA, 2018.
18. Bhaduri, S.; Contino, F.; Jeanmart, H.; Breuer, E. The effects of biomass syngas composition, moisture, tar loading and operating conditions on the combustion of a tar-tolerant HCCI (Homogeneous Charge Compression Ignition) engine. *Energy* **2015**, *87*, 289–302. [CrossRef]
19. Nadaleti, W.C.; Przybyla, G. Emissions and performance of a spark-ignition gas engine generator operating with hydrogen-rich syngas, methane and biogas blends for application in southern Brazilian rice industries. *Energy* **2018**, *154*, 38–51. [CrossRef]
20. Park, H.; Lee, J.; Jamsran, N.; Oh, S.; Kim, C.; Lee, Y.; Kang, K. Comparative assessment of stoichiometric and lean combustion modes in boosted spark-ignition engine fueled with syngas. *Energy Convers. Manag.* **2021**, *239*, 114224. [CrossRef]
21. Gobbato, P.; Masi, M.; De Simio, L.; Iannaccone, S. A method for determining hydrogen–methane–nitrogen mixtures for laboratory tests of syngas-fuelled internal combustion engines. *Int. J. Engine Res.* **2021**, *22*, 2533–2547. [CrossRef]
22. Tahtouh, T.; Halter, F.; Samson, E.; Mounaim-Rousselle, C. Effects of hydrogen addition and nitrogen dilution on the laminar flame characteristics of premixed methane–air flames. *J. Hydrog. Energy* **2009**, *34*, 8329–8338. [CrossRef]
23. Coppens, F.H.V.; De Ruyck, J.; Konnov, A.A. The effects of composition on burning velocity and nitric oxide formation in laminar premixed flames of CH_4+H_2+O_2+N_2. *Combust. Flame* **2007**, *149*, 409–417. [CrossRef]
24. Bika, A.S.; Franklin, L.; Kittelson, D.B. Engine knock and combustion characteristics of a spark ignition engine operating with varying hydrogen and carbon monoxide proportions. *J. Hydrog. Energy* **2011**, *36*, 5143–5152. [CrossRef]
25. Li, H.; Karim, G.A. Experimental Investigation of the Knock and Combustion Characteristics of CH_4, H_2, CO, and Some of Their Mixtures. *Proc. Inst. Mech. Eng. Part A J. Power Energy* **2006**, *220*, 459–471. [CrossRef]
26. Malenshek, M.; Olsen, D.B. Methane number testing of alternative gaseous fuels. *Fuel* **2009**, *88*, 650–656. [CrossRef]
27. Arunachalam, A.; Olsen, D.B. Experimental evaluation of knock characteristics of producer gas. *Biomass Bioenergy* **2012**, *37*, 169–176. [CrossRef]